JMEPEG (2009) 18:655–663
DOI: 10.1007/s11665-009-9375-0

1059-9495/$19.00

Study of a Nitinol Stent Deployed into Anatomically Accurate Artery Geometry and Subjected to Realistic Service Loading

Nuno Rebelo, Rachel Fu, and Michael Lawrenchuk

(Submitted September 12, 2008; in revised form December 4, 2008)

Realistic simulation of a stent in service loading is necessary for the design of Nitinol stents. This type of analysis is complicated by several issues: artery geometry and material properties are largely unknown and may vary from person to person; the loading on the stent is due to interactions between pulsatile blood flow, the artery, and stent. This study addresses the first issue by obtaining realistic artery geometry from magnetic resonance imaging (MRI) scans of a patient in the fetal and supine positions, and comparing deformation of the stent deployed into the two different artery configurations. The second issue is addressed by investigating two different methods of applying service loading. The first method applies sinusoidal pressure waves directly to the artery wall. The second method considers the effect of blood flow within the artery by performing a fluid-structure interaction (FSI) simulation. Simulation of expansion, annealing, crimping, and deployment of a Nitinol stent into the two artery configurations was performed using Abaqus. Following the deployment, sinusoidal pressure pulses, emulating systolic and diastolic blood pressures, were applied to the inner surface of the artery. To simulate the effect of blood within the artery, the coupled Eulerian-Lagrangian method in Abaqus was used. The blood was modeled as a partially filled Eulerian domain, whose material boundary contacted the Lagrangian artery. Transient inlet velocity and outlet pressure conditions were applied to the Eulerian domain to simulate blood flow. Since fatigue life calculations are important for the design of Nitinol stents, the maximum principal strains at the diastolic pressure troughs and the difference between the maximum principal strains at diastolic and systolic pressure were investigated for five cycles. Different maximum principal strains resulted for the different artery geometries (fetal or supine), while the difference between maximum principal strains was similar. For the simulations including the effect of blood flow, the maximum principal strains at the diastolic pressure troughs were somewhat higher than the simulations in which pressure was directly applied to the artery. In conclusion, this study established and compared various methods of improving the service loading in the simulation of Nitinol stents, specifically including anatomically correct artery geometry and the effect of blood flow.

Keywords biomaterials, modeling processes, titanium

1. Background/Objectives

The objective of this study is to demonstrate finite element analysis (FEA) methodologies which can be used to simulate the service loading on a Nitinol self-expanding stent with a more realistic approach than typical methods. The cyclic loading on a stent deployed into an artery is due to complex interactions between the pulsatile blood flow, the deformable artery, and the stent. In general, the loading is modeled using an expanding and contracting rigid cylinder in contact with the inner and outer surfaces of the stent (Ref 1, 2). This approximation does not account for the nonuniform deformation in the artery due to the pressure pulses, which is the main cause of the loading experienced by the stent. For this study, the stent was first deployed into a deformable artery, whose geometry was determined from MRI scans of a patient in both the supine and fetal positions. The interior surface of the artery was then subjected to systolic and diastolic pressure wave loading and the strains in the stent were compared for the two artery configurations. Finally, to examine the effect of blood flow within the supine artery, a coupled Eulerian-Lagrangian (CEL) analysis was performed in which blood contained within the artery was subjected to transient inlet velocity and outlet pressure conditions. The deformations and strains from this FSI analysis were then compared with those of the purely structural analysis.

This article is an invited paper selected from presentations at Shape Memory and Superelastic Technologies 2008, held September 21-25, 2008, in Stressa, Italy, and has been expanded from the original presentation.

Nuno Rebelo and **Rachel Fu**, DS Simulia Corp, SIMULIA Western Region, 39221 Paseo Padre Parkway, Suite F, Fremont, CA 94538; and **Michael Lawrenchuk**, Materialise, 6111 Jackson Rd., Ann Arbor, MI 48103. Contact e-mail: Nuno.Rebelo@3ds.com.

2. Methodology

The RESIStent consortium, working to improve the durability of Nitinol stents (Ref 3), produced a wealth of medical images of patients' superior femoral arteries (SFA). We have

used a sample of these in order to create a realistic environment into which a stent was deployed. Mimics software (Materialise, Ann Arbor, MI) was used to obtain the artery geometry utilized in this study. The artery geometry was isolated from the MRI data through semi-automated segmentation and surface modeling techniques. A gray value threshold was used to differentiate the artery from surrounding tissues, and some further editing was applied to create the initial artery geometry. The Mimics FEA Module was then used to optimize the surface mesh and facilitate the link with Abaqus (SIMULIA, Providence, RI). The artery model was then exported as a surface mesh to Abaqus. The procedure was performed for MRI scans of a patient in both the fetal and supine positions. Figure 1 shows the contrast MRI images in both positions as well as the corresponding FEA geometry generated. Because the simulations performed in this study pertain to stent deployment, only a small section of the artery was included in the FEA models, as shown in Fig. 1.

Abaqus was used as the FEA solver in this study. The stent design was laser-cut from a Nitinol tube with an outer diameter of 1.47 mm and a thickness of 0.216 mm. The stent mesh consisted of 114,561 linear hexahedral reduced integration elements. The material model for Nitinol behavior, built into Abaqus and based on the Auricchio and Taylor (Ref 4, 5) model was used. It included different behavior in tension and compression, different moduli for austenite and martensite, and transformation plateaus determined at body temperature. The artery was modeled with triangular shell elements of thickness and linear material properties as specified by Tittelbaugh et al. (Ref 6), in which the Young's modulus of the artery was calculated based on a compliance of 2.2%. All six degrees of freedom of the ends of the artery segments were modeled as fixed, and translational degrees of freedom of two points on one end of the stent were constrained to prevent rigid body motion.

Prior to any service loadings imposed on the stent, it was necessary to simulate the stent processing steps as well as the stent deployment into the artery. The first processing step modeled was the stent expansion from the as-cut configuration using a rigid surface to a specified inner diameter of 5.54 mm for the straight artery section (supine) and 6.56 mm for the bent artery section (fetal). The deviation from the rated stent expansion for this design was contrived in order for the stent to self-expand beyond the artery section. It should be noted that in principle, a stent would not be deployed into a bent SFA. A bent configuration would rather be obtained by bending both artery and stent after implantation into a straight configuration. Since the mechanical description of such deformations is not well characterized at this time, we have opted to deploy into a geometrically well-characterized bent configuration. Although not realistic, the procedure may yield interesting information about what happens when a self-expanding stent is deployed into a curved artery. The annealing step was then modeled by removing the stent elements and adding them back into the model in a strain free manner. The final processing step modeled was the crimping of the stent using a rigid surface to an outer diameter of 3.30 mm. The crimped stent was then released into either the bent or straight artery sections through removal of contact with the rigid surface. The deformation at each of these steps is shown in Fig. 2. These simulation steps were performed in Abaqus/Standard as static analyses.

It is well known that average blood pressure fluctuates between a systolic value of 120 mmHg (15,999 Pa) and a diastolic value of 80 mmHg (10,666 Pa) with a mean value of 100 mmHg (13,332 Pa). Since the artery geometry was obtained in vivo, it corresponds to a deformation state which accounts for the mean internal pressure of 100 mmHg. Therefore, to simulate systolic and diastolic fluctuations, a sinusoidal pressure wave fluctuating between 20 mmHg

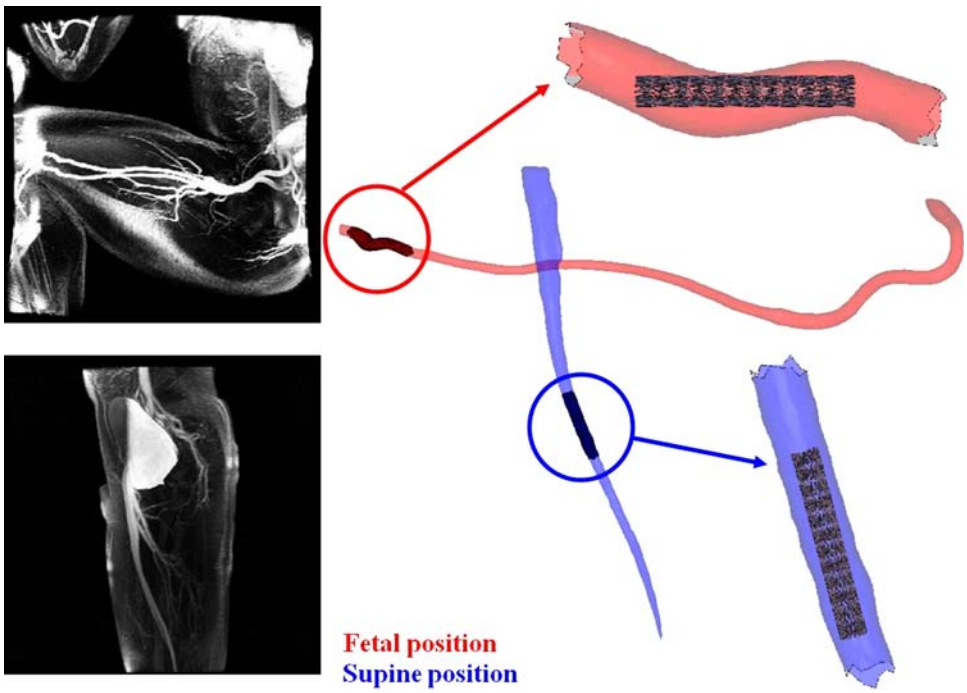

Fig. 1 Femoral artery geometry including the MRI scan in fetal (*upper*) and supine (*lower*) positions and the FEA geometry segments modeled (stent prior to deployment shown)

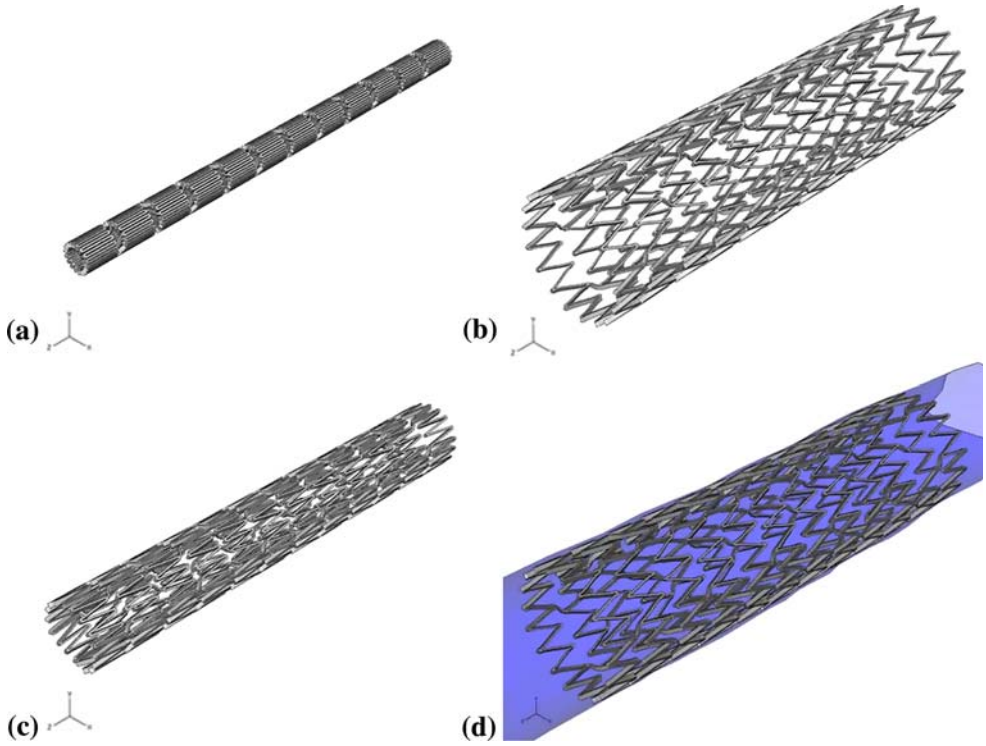

Fig. 2 Analysis steps prior to service loading (a) laser-cut stent, (b) expanded, (c), crimped, and (d) deployed into artery

(2666 Pa) and −20 mmHg (−2666 Pa) was applied to the inner artery surface at a frequency of 1.2 Hz, and five cycles were modeled. Tittelbaugh et al. (Ref 6) showed that for this frequency, dynamic effects are negligible, so the pressure loading was also modeled as a static procedure.

For the next step in realistic service loading, we wished to investigate the effect of the blood flow within the artery, as it is the contact pressure exerted by the fluid which is actually causing the structural loading. Abaqus/Explicit contains an Eulerian capability to complement and interact with the traditional Lagrangian analysis. In a Lagrangian analysis, nodes are fixed within the material and the elements deform as the material deforms; in an Eulerian analysis, nodes are fixed in space and material flows through elements that do not deform (Ref 7). Since Eulerian elements may be partially filled with or completely void of material, the Eulerian material boundary is computed during each time increment using a volume of fluid formulation. Eulerian-Lagrangian contact allows Eulerian material to interact with Lagrangian elements, enabling simulation of FSI.

The main advantage of the CEL method is that FSI analyses can be performed within the same model using a single analysis code. Other methods of FSI generally involve transferring loads and boundary conditions between simultaneous structural and computational fluid mechanics models, requiring multiple analysis codes as well as a means of information transfer between the two codes.

Because the Eulerian capability has been implemented in Abaqus/Explicit, the CEL method is most suitable for high-speed dynamic events. However, because the period of pulsatile blood flow is approximately 1 s, various modeling techniques were required to obtain a solution from the Explicit solver within a reasonable amount of solution time. The integration operator in the explicit procedure is conditionally stable, so incrementation is controlled by a stable time increment calculated by the solver.

Figure 3 shows the model setup of the coupled FSI model. The stress state and deformed configuration of the stent released into the straight artery was imported into a model containing the definition of the Eulerian domain. The Eulerian domain consisted of 6804 elements and was initially specified as partially filled with material boundaries at the artery wall. The transient inlet velocity condition specified was determined from Fourier coefficients derived by Steinman et al. (Ref 8). The transient outlet pressure condition applied was as determined by Tittelbaugh et al. (Ref 6) from modeling a long length of vessel with the inlet velocity condition and a zero pressure outlet condition. The outlet pressure approximately fluctuates between positive and negative 20 mmHg (2666 Pa). The inlet velocity and outlet pressure profiles are also shown in Fig. 3. Note that because the elements in the Eulerian domain are larger than the elements in the stent, contact between the stent and the blood was not included. It was assumed that the driving load on the stent is the artery motion. Mesh refinement of the Eulerian domain would be required to capture the flow details between the struts of the stent; however, such an analysis would become considerably more expensive in computational terms.

Blood was modeled using the linear Us-Up Hugoniot form equation of state (EOS) material model. This type of material model determines the pressure as a function of density and specific energy. Blood density was specified to be the same as water (983 kg/m^3) and additionally, EOS shear viscosity was specified to be approximately three times that of water (0.003 Pa s). The speed of sound in blood was calculated to

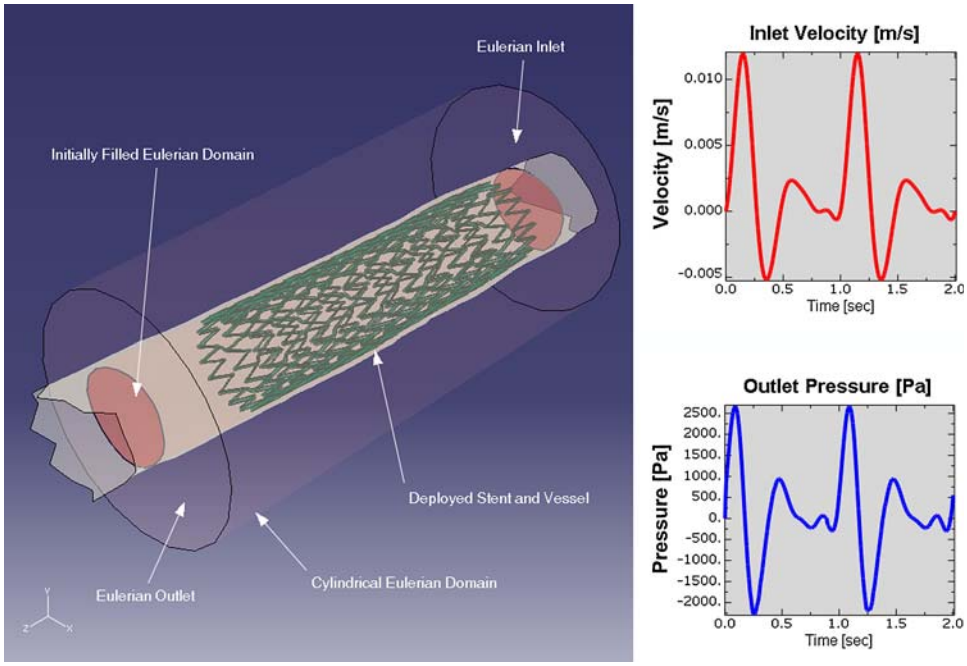

Fig. 3 Coupled Eulerian-Lagrangian model setup and transient inlet velocity and outlet pressure profiles

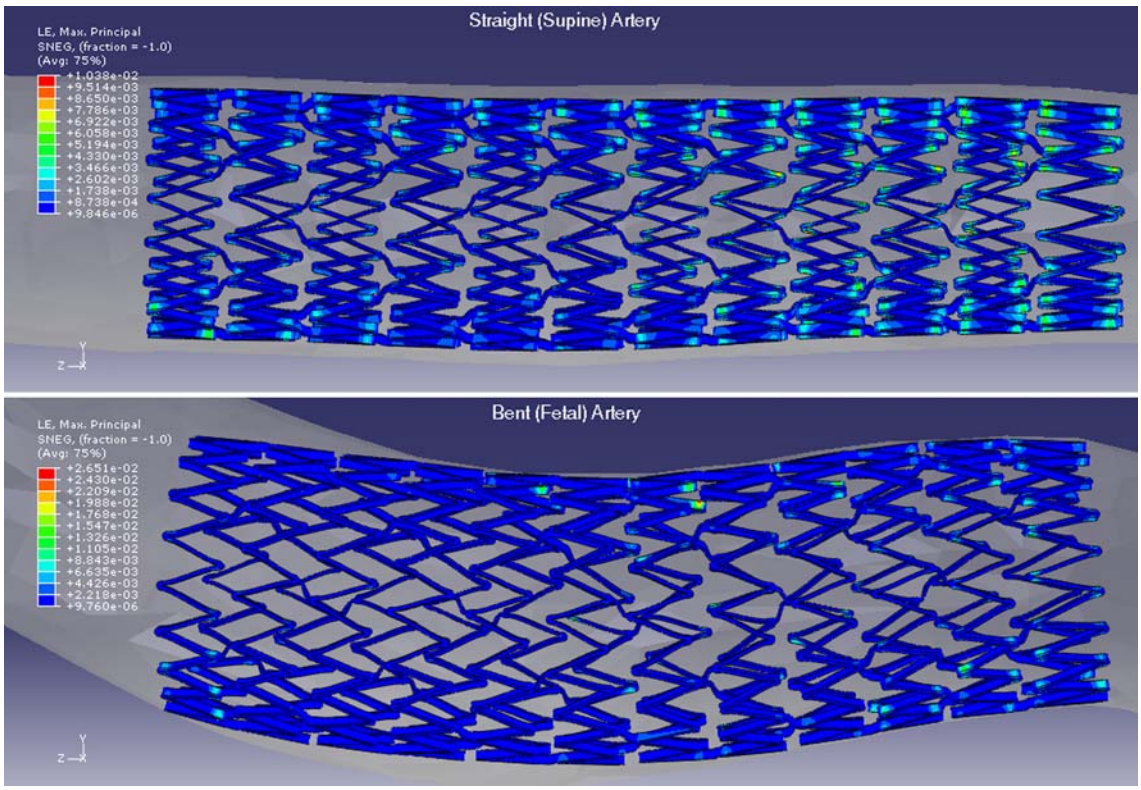

Fig. 4 Maximum principal strains of the fully deployed stent in the straight and the bent artery sections

be 1450 m/s. For EOS materials, the stable time increment is inversely proportional to the speed of sound in the material, and for nearly incompressible fluids such as blood, the stable time increment can be very small. Decreasing the speed of sound increases the stable time increment, but also increases the compressibility of the fluid.

3. Results

The stent configuration after deployment into both the straight and bent artery sections is shown in Fig. 4. The stent deployed into the bent artery section does not have enough

flexibility to make full contact with the artery wall at all locations, and so may be less effective than a stent deployed into a straight artery section. Figure 4 also shows that the peak maximum principal strain value in the fully deployed stent is more than double in the bent artery section.

The maximum principal strains of the stent subjected to cyclic loading are generally of interest for fatigue life calculations. For the sinusoidal pressure loading applied to the artery, the maximum principal strain in the stent will occur at the diastolic pressure trough, and these results are shown for the straight and bent artery sections on the left side of Fig. 5 and 6, respectively. Since the stent generally takes the first cycle to settle, only results from the second to fifth cycles are shown. The change in maximum principal strains between the diastolic and systolic pressure peaks and troughs is also required for fatigue life calculations, and are also shown on the right side of Fig. 5 and 6. The cyclic evolution of results is due to the nonlinear material behavior and to contact conditions as well. No changes in material behavior properties with cycling were taken into account in this study.

As expected, for both the bent and straight artery sections, the maximum principal strains decrease with cycling until approximately steady values are achieved. The peak maximum principal strains in the stent deployed into the bent artery section are approximately three times higher than in the straight section, highlighting the importance of utilizing accurate artery geometry of the location of deployment. The higher maximum principal strains in the stent deployed into the bent artery section may indicate that the contrived expansion radius may have been sized incorrectly.

For the stent in both the bent and straight artery sections, the delta maximum principal strains are similar for all cycles modeled, and are also similar between the straight and bent artery segments. This is reasonable, since the same pressure fluctuations were applied to the bent and straight arteries.

As previously mentioned, because the CEL capability is available in Abaqus/Explicit, approximations were made to obtain a solution in a reasonable amount of analysis time. First, the wave speed of blood was specified to be one order of magnitude lower than actual, to increase the stable time increment. Second, the period of the inlet velocity and outlet pressure cycles was decreased from 1 to 0.01 s. Simplified CEL analyses of the blood and artery without the stent were run to investigate the validity of these assumptions.

Because decreasing the wave speed of blood increases the compressibility, the main consequence for this application would be a decrease in contact pressure between the blood and artery. A simplified CEL analysis in which the fluid inlet and outlet were pressurized to 5333 Pa was compared with a structural analysis in which a pressure of 5333 Pa was directly applied to the artery. Figure 7 shows that the artery deformations are very similar for these two cases, indicating that the lower wave speed does not significantly affect contact pressures between the blood and the artery. Figure 7 also shows that the maximum increase in density in the blood is below 0.5%, so the fluid behavior is still close to incompressible, even with the reduced wave speed.

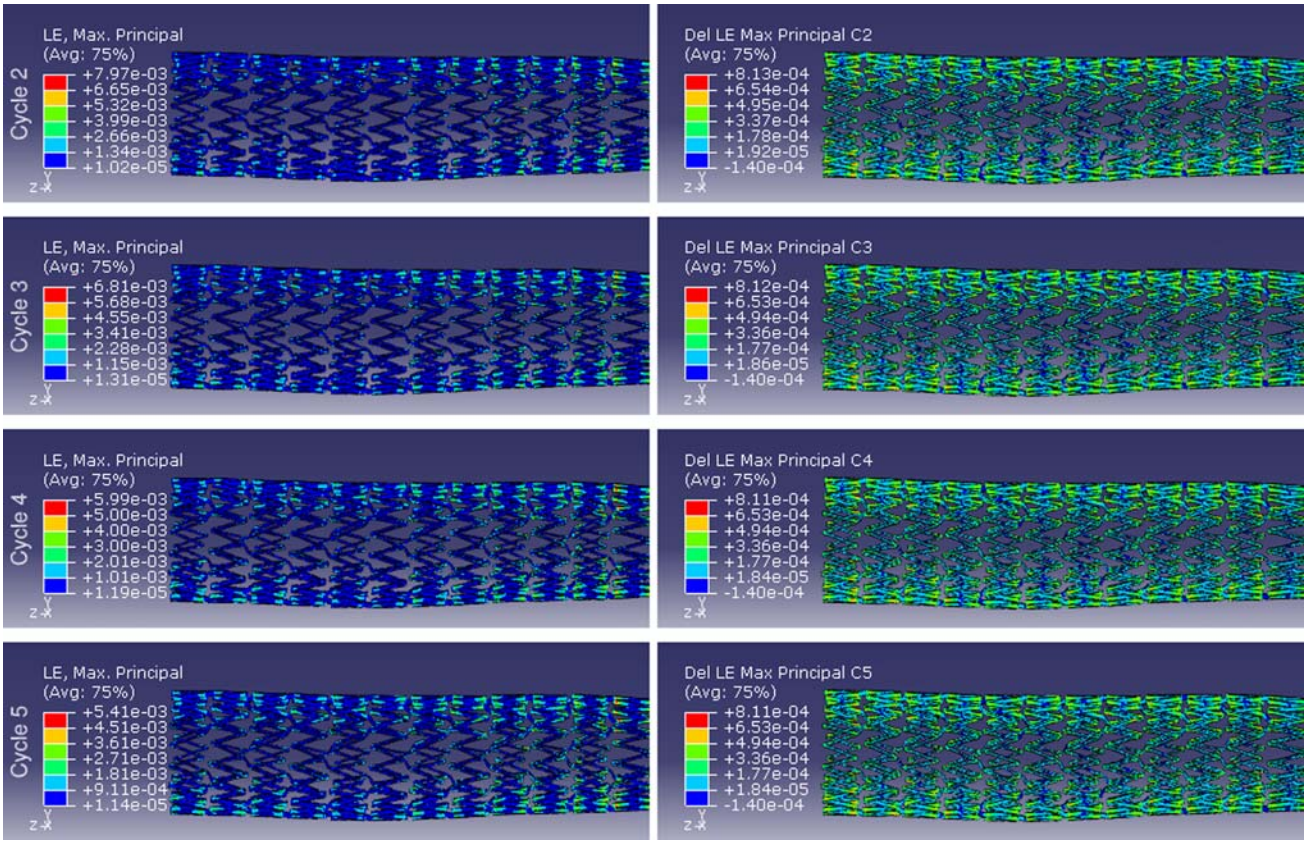

Fig. 5 Maximum principal strains at diastolic pressure (*left*) and delta maximum principal strains between diastolic and systolic (*right*) in the straight artery segment for the second to fifth cycles

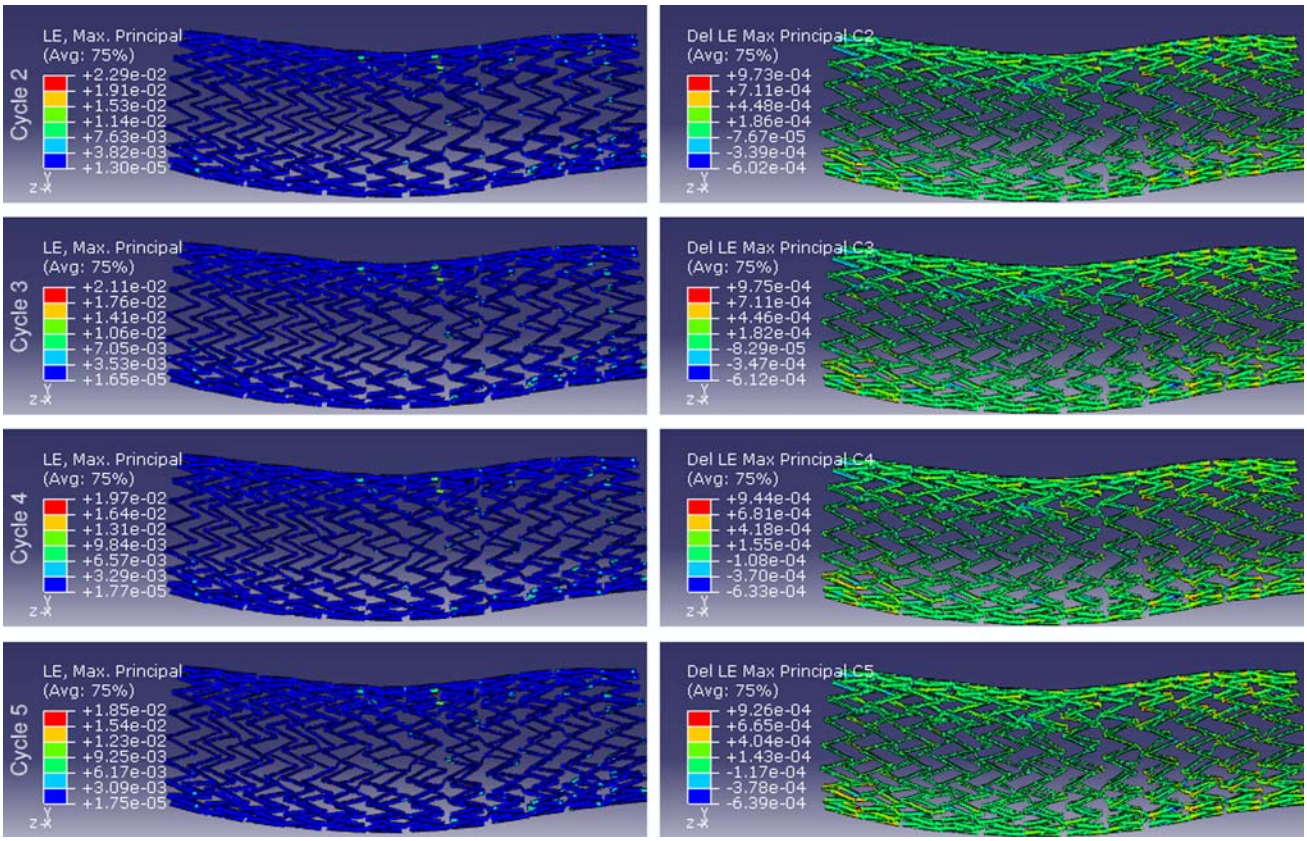

Fig. 6 Maximum principal strains at diastolic pressure (*left*) and delta maximum principal strains between diastolic and systolic (*right*) in the bent artery segment for the second to fifth cycles

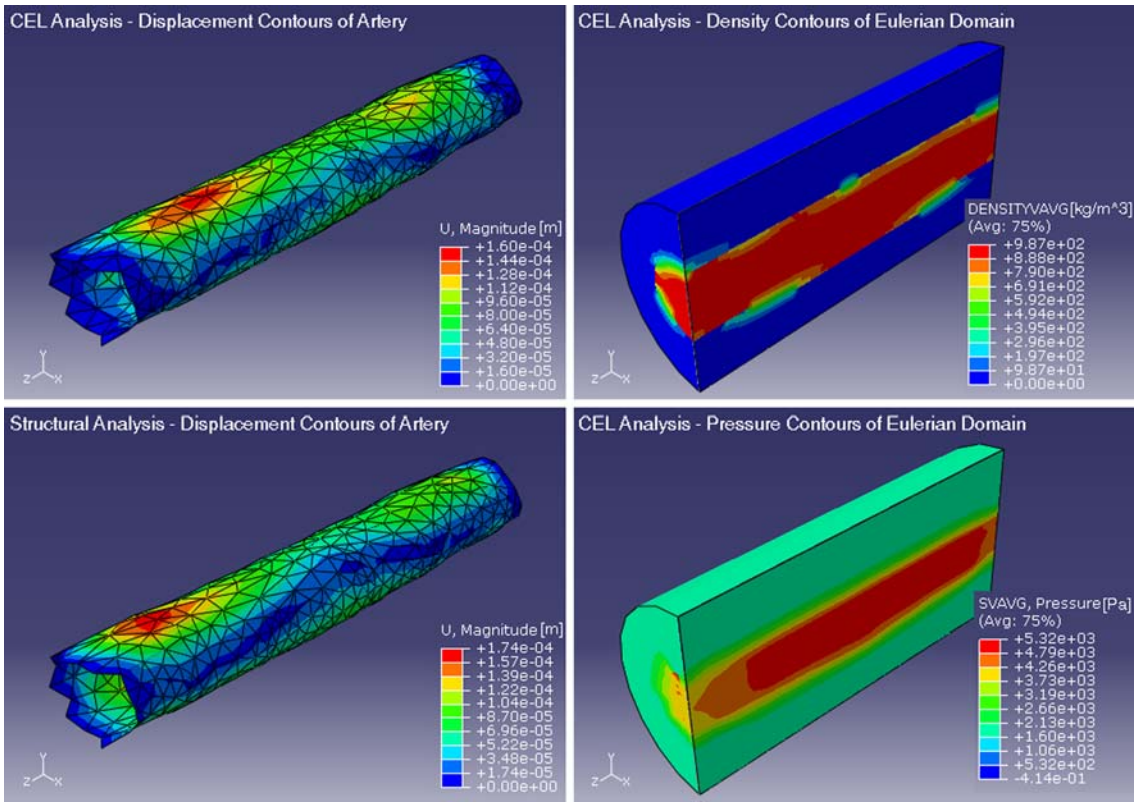

Fig. 7 Deformation contours of the artery for pressure directly applied to the artery and for the simplified CEL model; density and pressure contours for the simplified CEL model

The kinetic energy was compared with the internal energy for a simplified CEL analysis with the inlet velocity and outlet pressure cycles accelerated to reduce computation time. Figure 8 shows that the ratio of kinetic energy (ALLKE) to internal energy (ALLIE) in the model fluctuates about an average of approximately 3.5%, indicating that the higher frequency of the inlet velocity and outlet pressure cycles still yields reasonably quasi-static results.

Figure 9 shows the transient velocity vectors and pressure contours of a mid-plane cut through the Eulerian domain for the fifth cycle of the full CEL analysis. The outline of the artery is also shown to indicate the Eulerian material boundary location. These results show a parabolic flow distribution as expected; however, the outlet pressure condition generates a backflow at the systolic peak. This may indicate that the phase difference between the periodic velocity and pressure

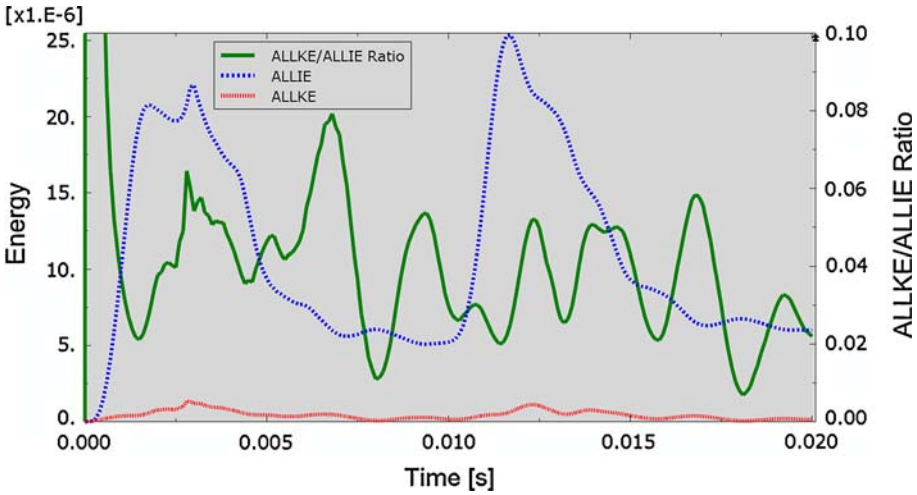

Fig. 8 Kinetic (ALLKE) and internal (ALLIE) energy results for the simplified CEL model

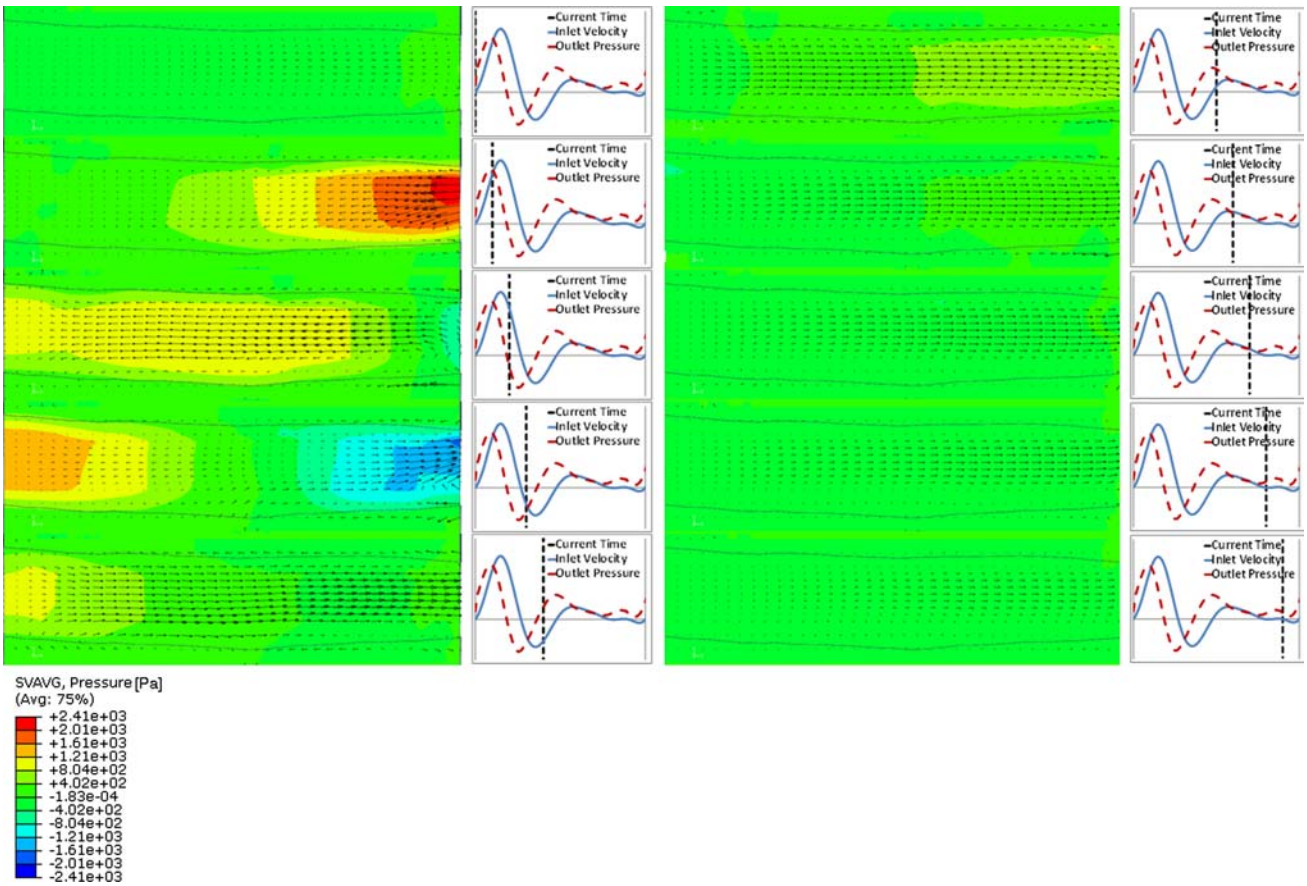

Fig. 9 Pressure contours and velocity vectors of blood in the full CEL model during the fifth cycle

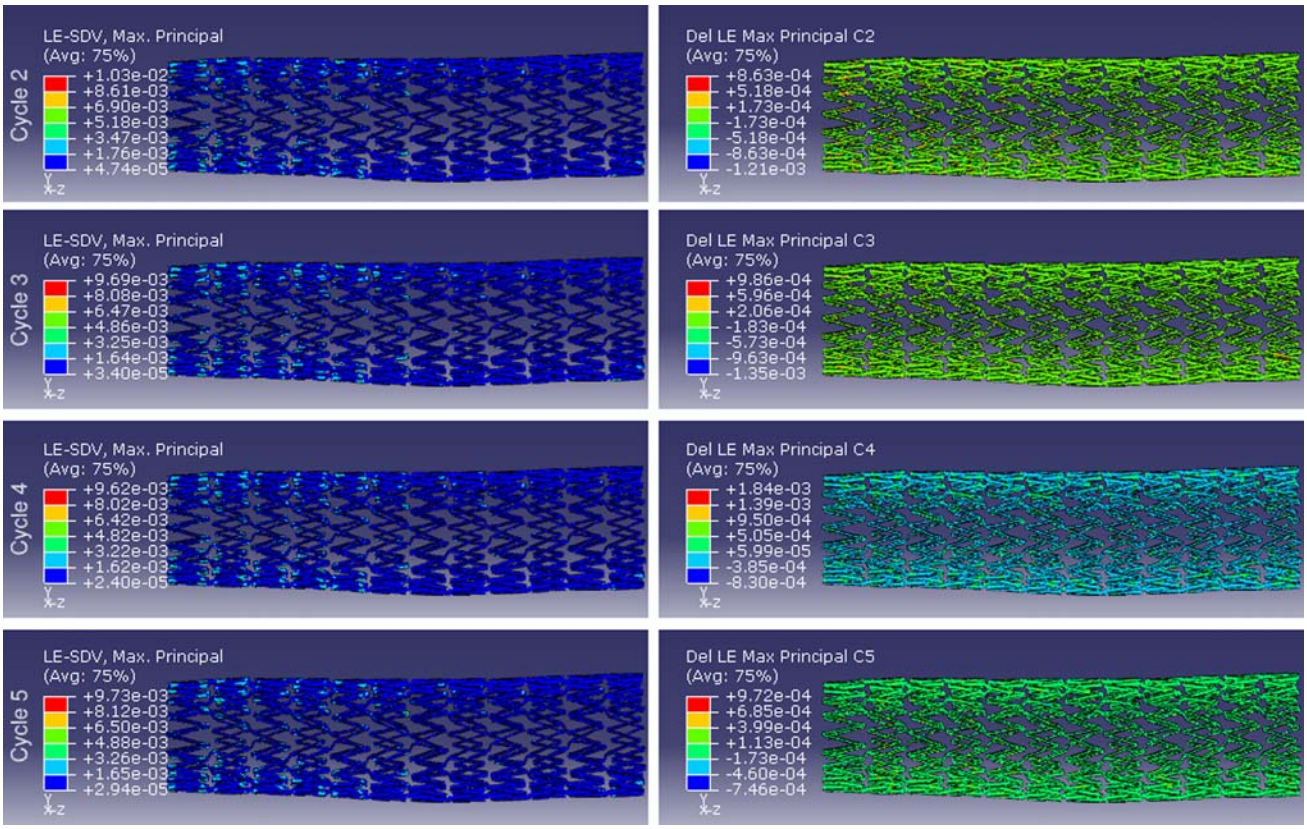

Fig. 10 Maximum principal strains at diastolic pressure (*left*) and delta maximum principal strains between diastolic and systolic (*right*) from the full CEL model for the second to fifth cycles

conditions may not be appropriate for the length of artery modeled in this study.

For the full CEL model, the systolic peak and diastolic trough are defined by the peak and trough of the transient outlet pressure condition. Figure 10 shows that the maximum principal strains in the stent at the diastolic troughs are somewhat higher for the CEL model than for the model in which pressure was directly applied to the artery. Differences are reasonable, and attributable to the fact that in the CEL model the pressure distribution is not uniform along the length of the artery. However, the difference in maximum principal strain between the systolic peak and diastolic trough is similar to the case with the pressure waves directly applied to the artery.

4. Discussion

Loading on the stent in the femoral artery is due to the pulsatile nature of blood flow, which can fluctuate about a mean pressure of 100 mmHg (13,332 Pa) with an amplitude of 20 mmHg (2666 Pa). Since the artery geometry was obtained in vivo, its deformation accounts for the mean pressure and only the pressure fluctuations need to be applied. Therefore, sinusoidal pressure waves were applied to the inner surface of the artery, and the resulting deformation of the stent was observed. The stent will experience maximum strains at the diastolic pressure trough, and typically the difference in maximum principal strains between the systolic peak and diastolic trough is used for fatigue life calculations. After five cycles, the largest maximum principal strain converged to approximately 0.5% in the stent deployed into the supine (straight) artery section and approximately 1.9% in the stent deployed into the fetal (bent) artery section. However, the maximum difference in maximum principal strains between systolic and diastolic is similar between 0.08% and 0.09%.

The CEL capability in Abaqus/Explicit was investigated to include the effects of blood flow within the supine artery on the stent deformation. Loading and boundary conditions become even more difficult to ascertain. Transient inlet velocity and outlet pressure conditions were specified on the Eulerian domain. Since Abaqus/Explicit is ideally suited for high-speed dynamic events, approximations were made to obtain results in a reasonable amount of time: reducing the wave speed of the fluid and decreasing the period of the cyclic velocity and pressure loading. Using a simplified CEL model which included only the blood and the artery, these assumptions were shown to yield reasonable results.

For the CEL model with the stent deployed into the supine artery, the peak maximum principal strain converged to approximately 0.97% in five cycles, which is slightly higher than the model with the pressure directly applied to the artery. The peak difference in maximum principal strains between systolic and diastolic is approximately 0.1%, which is similar to the values obtained with the pressure directly applied to the artery.

The original intent of investigating the stent deployed into the bent or fetal artery section was to ascertain the stent deformation changes when the patient shifts from the supine to the fetal position. The method in this study of deploying the stent into the bent artery section is only an approximation of this event, and future work would involve determining a more accurate method to simulate the shift.

For the CEL model in this study, backflow at the outlet during the systolic pressure peak indicated that the phase difference between the transient inlet velocity and outlet pressure may not be appropriate for the length of artery modeled. A partially blocked outlet to induce back pressure or an experimentally determined pressure condition could be investigated in future work. Also, the Eulerian mesh could be refined so that contact between the blood and stent could be included. Still, this study has demonstrated a method of FSI analysis which includes the effects of blood flow in simulating service loading of a stent deployed into an anatomically correct artery geometry.

References

1. N. Rebelo and M. Perry, Finite Element Analysis for the Design of Nitinol Medical Devices, *Min. Invas. Ther. Allied Technol.*, 2000, **9**(2), p 75–80
2. N. Rebelo, S. Prabhu, C. Feezor, and A. Denison, Deployment of a Self-Expanding Stent in an Artery, *Proceedings of the International Conference on Shape Memory and Superelastic Technologies* (Kurhaus Baden-Baden, Baden-Baden, Germany), 2004
3. RESIStent Program: SRI International, Stanford University and a Consortium of Stent Manufacturers, 2004-2006, private communication
4. F. Auricchio and R. Taylor, Shape-Memory Alloys: Modeling and Numerical Simulations of the Finite-Strain Superelastic Behavior, *Comput. Meth. Appl. Mech. Eng.*, 1996, **143**, p 175–194
5. F. Auricchio and R. Taylor, Shape-Memory Alloys: Macromodeling and Numerical Simulations of the Superelastic Behavior, *Comput. Meth. Appl. Mech. Eng.*, 1997, **146**, p 281–312
6. E.M. Tittelbaugh, R. Fu, and S. Sett, Coupling FEA to CFD to Investigate the Effects of Pulsatile Blood Flow on the Dilatation of Artery Walls, *Proceedings of the NAFEMS World Congress* (Vancouver, BC, Canada), 2007
7. Dassault Systemes SIMULIA Corp., *Abaqus User's Manual 6.8*, Providence, Rhode Island, 2008
8. D. Steinman, B. Vinh, C. Ethier, M. Ojha, R. Cobbold, and K. Johnston, A Numerical Simulation of Flow in a Two-Dimensional End-to-Side Anastomosis Model, *J. Biomed. Eng.*, 1993, **115**, p 112–118